Electronic Supplementary Material

Promoting Water Reduction Reaction of Transition Metal Dichalcogenides in Basic Electrolyte by Interface Engineering

Hui Ding,[a] Qiyang Jiao,[a] Haifeng Lv,[b] Kun Xu,[a] Qiyu Xing,[a] Min Chen,[a] Wangsheng Chu, [c] Xiaojun Wu,[b] Yuqiao Guo*[a]

[a] H. Ding, Q. Jiao, K. Xu, Q. Xing, M. Chen, Z. Hao, Y. Lin, Prof. Y. Q. Guo
Hefei National Laboratory for Physical Sciences at the Microscale,and iChEM (Collaborative Innovation Centre of Chemistry for Energy Materials), and School of Chemistry and Materials Science, University of Science and Technology of China, Hefei, Anhui 230026, P. R. China
*E-mail: guoyq@ustc.edu.cn

[b] H. Lv, Prof X. Wu
Department CAS Key Laboratory of Materials for Energy Conversion and Department of Material Science and Engineering University of Science and Technology of China, Hefei, Anhui 230029, P. R. China.

[c] Prof W. Chu
National Synchrotron Radiation Laboratory University of Science & Technology of China, Hefei, Anhui 230029, P. R. China.

Characterization

Powder X-ray Diffraction was conducted on Philips X'Pert Pro Super diffractometer with Cu Kα radiation (λ=1.54178 Å). The transmission electron microscopy (TEM) were performed on a JEOL-2010 at an acceleration voltage of 200 KV. The scanning electron microscopy (SEM) images were taken on a JEOL JSM-6700F SEM. The high-resolution TEM (HRTEM), high-angle annular dark-field scanning transmission electron microscopy (HAADF-STEM) images and STEM-EELS mapping images were taken on a JEOL JEM-ARF200F atomic resolution analytical microscope. Faradaic yield in H_2 generation, and the experimental results are obtained from gas chromatography measurements (Agilent 7890A). The Mo and Ni K edge absorption spectra were collected in transmission mode at the X-ray absorption fine structure (XAFS) station of the 1W1B beamline of the Beijing Synchrotron Radiation Facility (BSRF, Beijing).

Calculation

In our system, the $MoSe_2$ (101) is coaxially grown on the (101) surface of NiSe nanoplate. According to the symmetry of $MoSe_2$ and NiSe crystal, the side faces should be (001). As a result, the interface of this heterostructure is built with a tri-layered NiSe (001) as the substrate with the deposited $MoSe_2$ (001) nanoribbon. The $MoSe_2$ nanoribbon is built using a $2\times2\sqrt{3}$ supercell of $MoSe_2$ units with two border Se atoms (8 Mo atoms and 18 Se atoms). The lattice mismatch is within 3% and the system is free to relax with the bottom layer of NiSe is fixed. The active catalytic sites locate at the borders of $MoSe_2$ ribbons and the substrate can promote the dissociation process of water molecule. All first-principle calculations were performed with the density functional theory (DFT) method implemented in the Vienna Ab-initio Simulation Package (VASP) package [1-2]. The projector augmented wave (PAW) [3-4] pseudopotential and the Perdew-Burke-Ernzerhof (PBE) exchange-correlation functional [5] were used in the calculations with a 450 eV plane-wave cut-off energy. All calculations were spin-polarized and the lattice parameters were optimized until the convergence tolerance of force on each atom was smaller than 0.05 eV. The energy converge criteria was set to be 10-5 eV for self-consistent calculations with a gamma-center 4x4x1 k-mesh. All periodic slab models have a vacuum spacing of at least 15 Å.

Calculation details:

The key reaction steps in alkaline HER:

① $H_2O + e^- + cat \rightarrow H^*\text{-}cat + OH^-$ (Volmer step)

② $2H^*\text{-}cat \rightarrow H_2\uparrow$ (Tafel step)

③ $H^*\text{-}cat + H_2O + e^- \rightarrow cat + OH^- + H_2\uparrow$ (Heyrovsky step)

To avoid the computation of the exact free energy of OH^- in solutions, we assume the free energy for step ① and ③ are at the same equilibrium potential of HER. Therefore, the whole progress can be regarded as the four stages: initial state, activated water adsorption, H* intermediates formation, H_2 formation, which the free energies (at the reduction potentials $U_0 = 0$ V vs RHE) can be calculated as:

$$G_0 = G_{cat} + G_{H_2O}$$

$$G_1 = G_{cat\text{-}(H\text{-}OH)^*}$$

$$G_2 = G_{cat\text{-}H^*} + G_{OH^-}$$

$$G_3 = G_{cat} + G_{OH^-} + \frac{1}{2}G_{H_2}$$

and $G_3 = G_0$.

The free energies of every reaction step are provided in the Table S1.

Table S1. Thermodynamic data used in the free energy of formation calculations. CS and HS represent the clean surface and the hetero-structured NiSe/$MoSe_2$.

Species	ZPE(eV)	TS(eV)	E(eV)
H_2O	0.56	0.67	-14.23
H_2	0.27	0.41	-6.76
$MoSe_2$_CS	0	0	-168.41
(HO-H)*-$MoSe_2$	0.51	0.16	-182
H*-$MoSe_2$	0.2	0.01	-172.35
$MoSe_2$/NiSe	0	0	-578.51
(HO-H)*-$MoSe_2$/NiSe	0.56	0.20	-593.12
H^*-$MoSe_2$/NiSe	0.21	0.02	-582.36

Here, the free energy was calculated using the equation:

$$G = E + ZPE - TS$$

where G, E, ZPE and TS are the free energy, total energy from DFT calculations, zero-point energy and entropic contributions (T was set to be 300K), respectively. ZPE could be derived after frequency calculation by:

$$ZPE = \frac{1}{2}\sum h\nu_i$$

TS values of H_2O and H_2 are from previous report [6]. And the TS values of adsorbed species are calculated after obtaining the vibrational frequencies [7]:

$$TS_\nu = k_B T\left[\sum\nolimits_K \ln\left(\frac{1}{1-e^{-h\nu/k_B T}}\right) + \sum\nolimits_K \frac{h\nu}{k_B T}\frac{1}{(e^{h\nu/k_B T}-1)} + 1\right]$$

Supplementary Figures

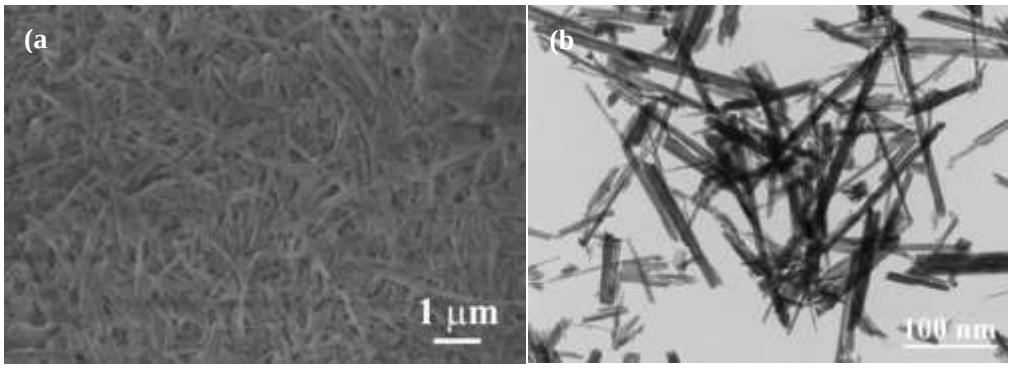

Figure S1. (a) SEM and (b) TEM images of $NiMoO_4$ precursor

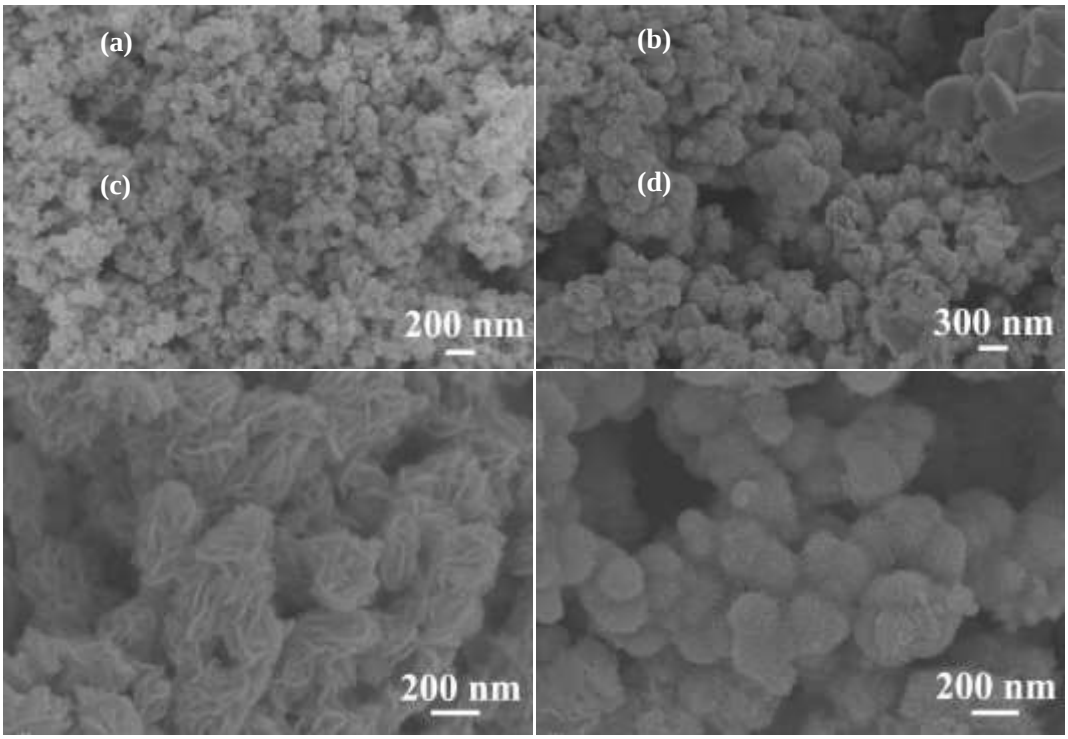

Figure S2. SEM images of (a) NiSe, (b) WC-NiSe/$MoSe_2$, (c) SC-NiSe/$MoSe_2$ and (d) $MoSe_2$.

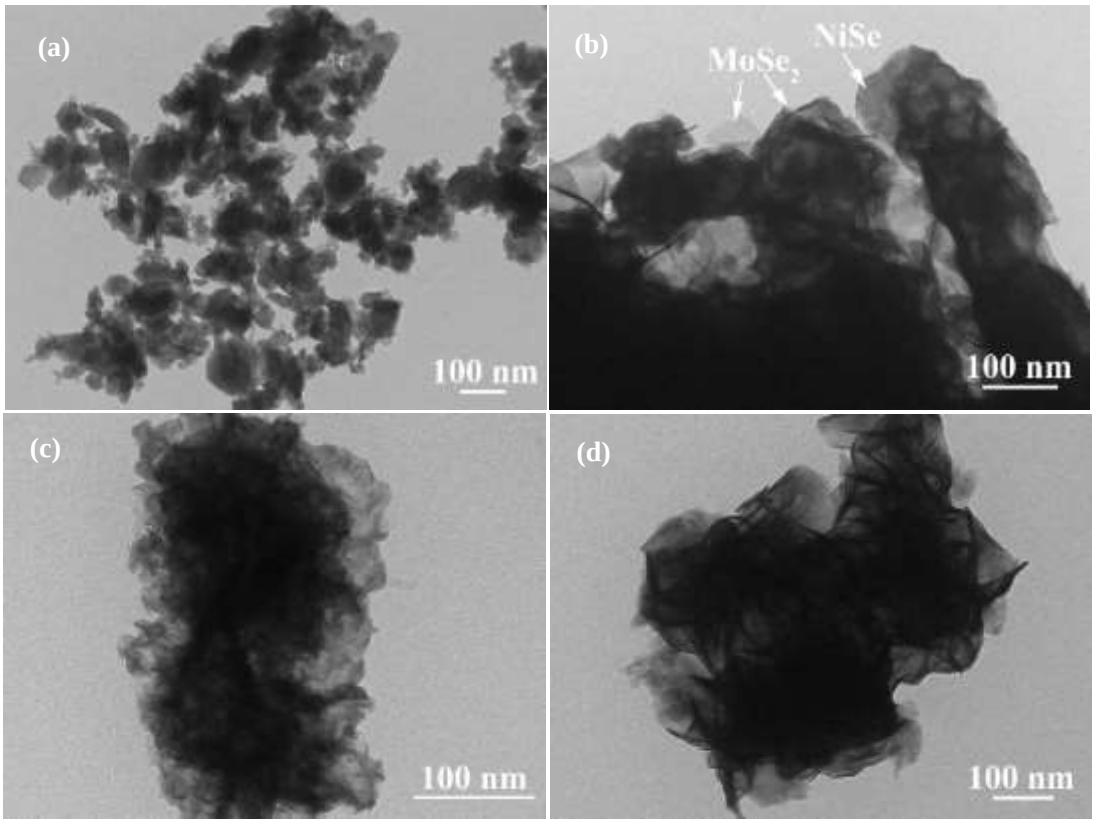

Figure S3. (a) TEM images of NiSe, (b) WC-NiSe/$MoSe_2$, (c) SC-NiSe/$MoSe_2$, and (d) $MoSe_2$

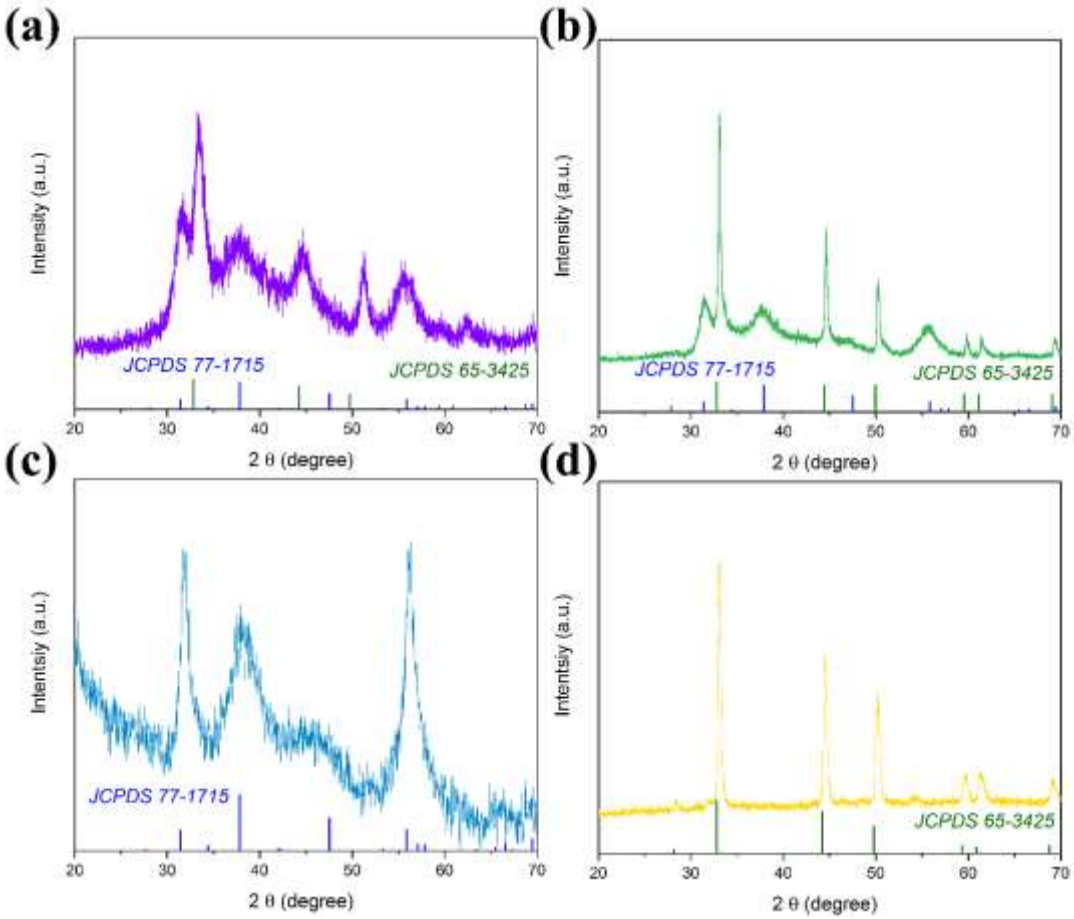

Figure S4. XRD patterns of (a). SC-NiSe/$MoSe_2$, (b). WC-NiSe/$MoSe_2$, (c). $MoSe_2$ and (d). NiSe. SC-NiSe/$MoSe_2$ and WC-NiSe/$MoSe_2$ are composed by NiSe and $MoSe_2$, both of which are hexagonal phase (Space group: P63/mmc (194)).

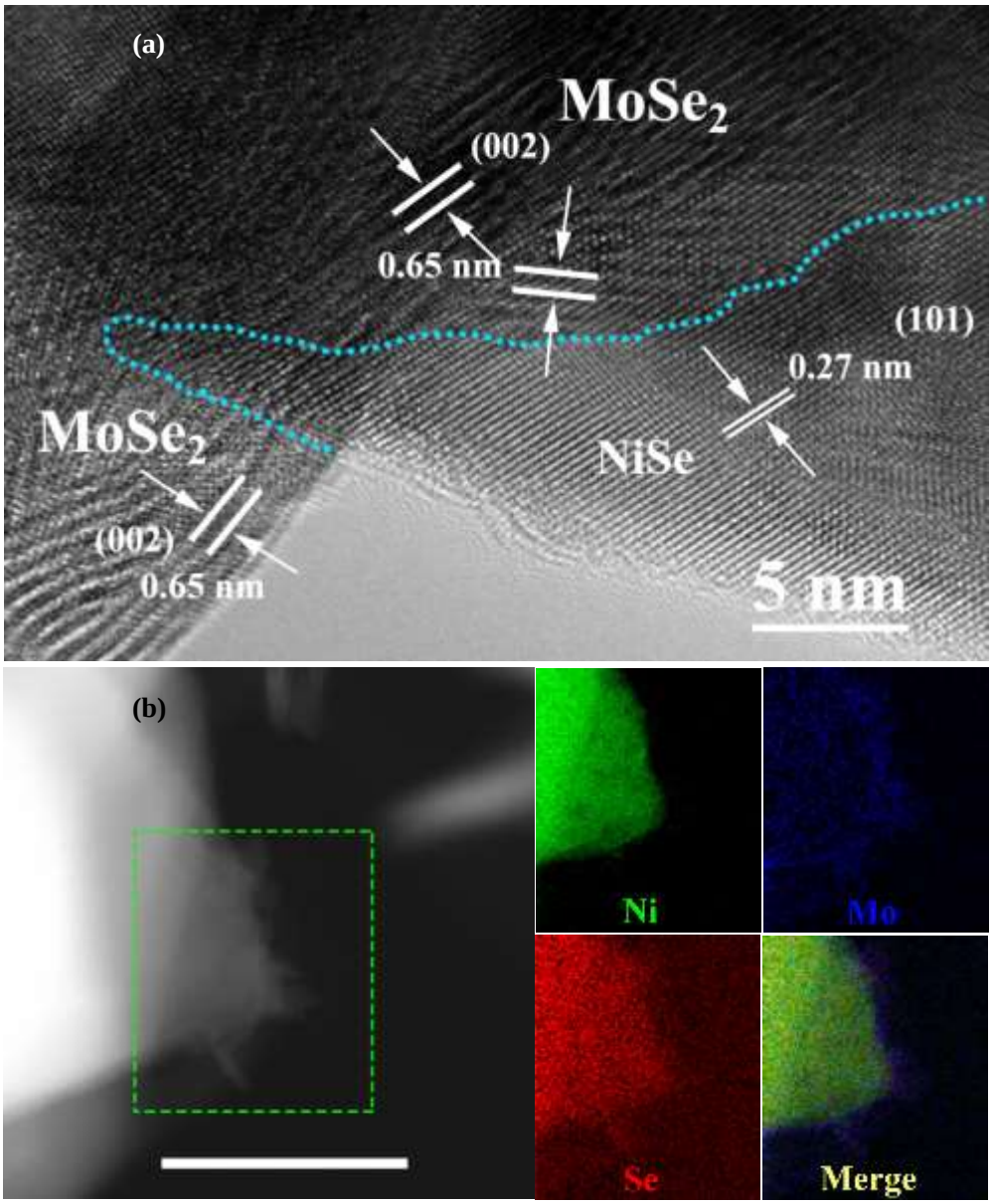

Figure S5. (a) HRTEM image of WC-NiSe/$MoSe_2$, (b) HADDF and corresponding EELS mapping images of WC-NiSe/$MoSe_2$. (Scale bar 50 nm). The Ni element is localized at nanoparticle shape area in WC-NiSe/$MoSe_2$, which shows different microstructure in contrast to SC-NiSe/$MoSe_2$.

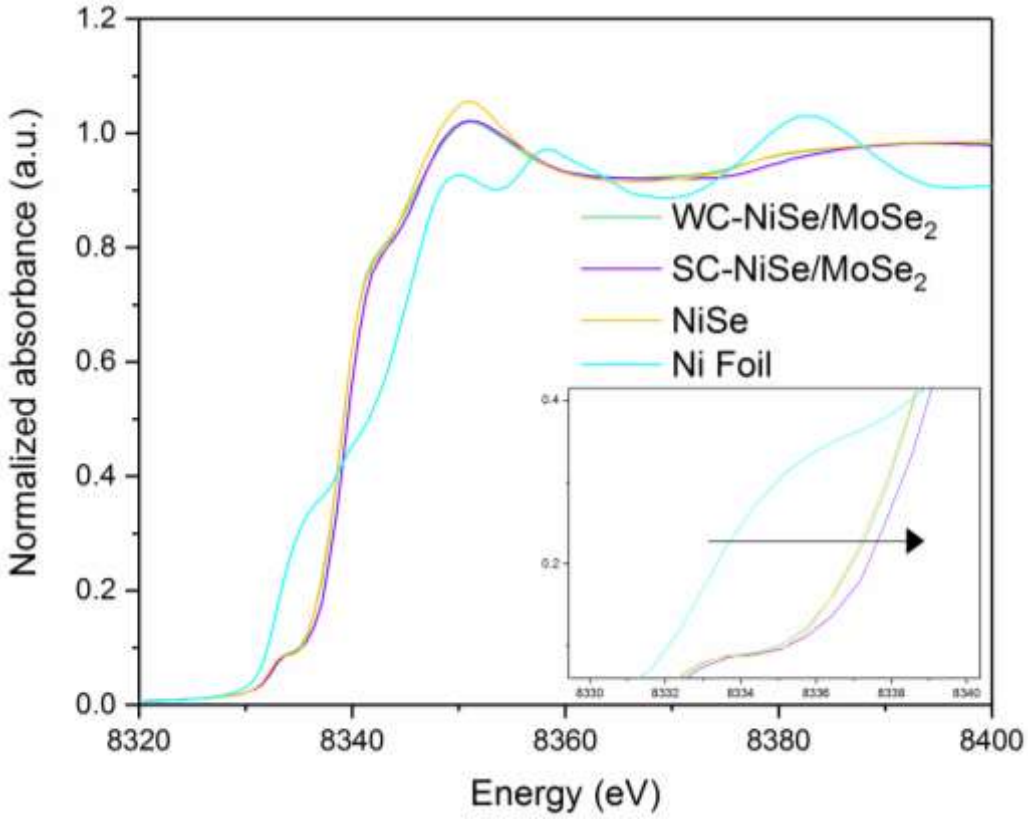

Figure S6. Ni K-edge XANES spectrums.

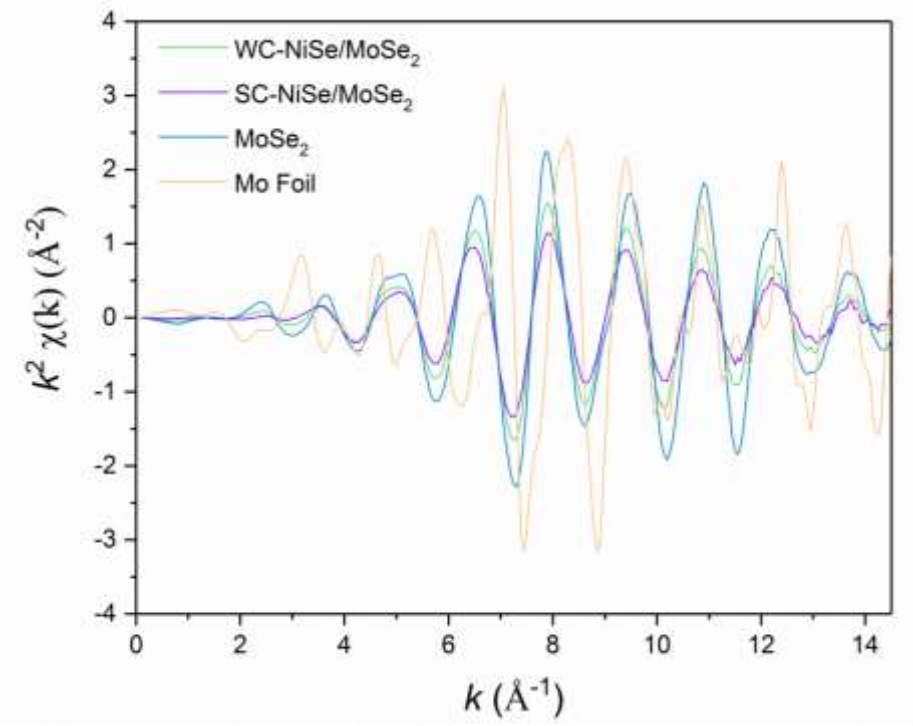

Figure S7. Mo K-edge extended EXAFS oscillation.

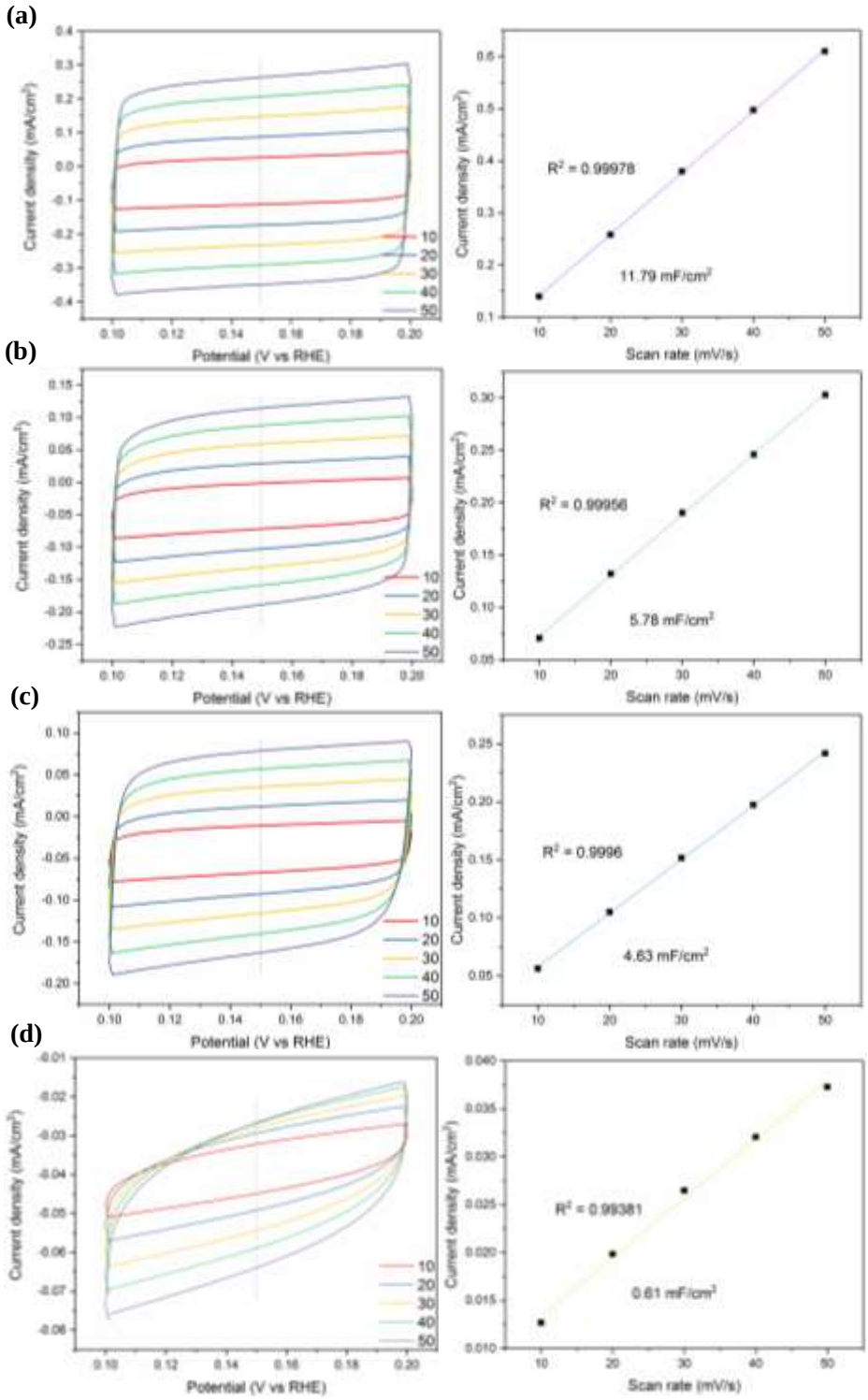

Figure S8. Cyclic voltammetry plots at different scan rate of (a) SC-NiSe/$MoSe_2$, (b) WC-NiSe/$MoSe_2$, (c) $MoSe_2$ and (d) NiSe

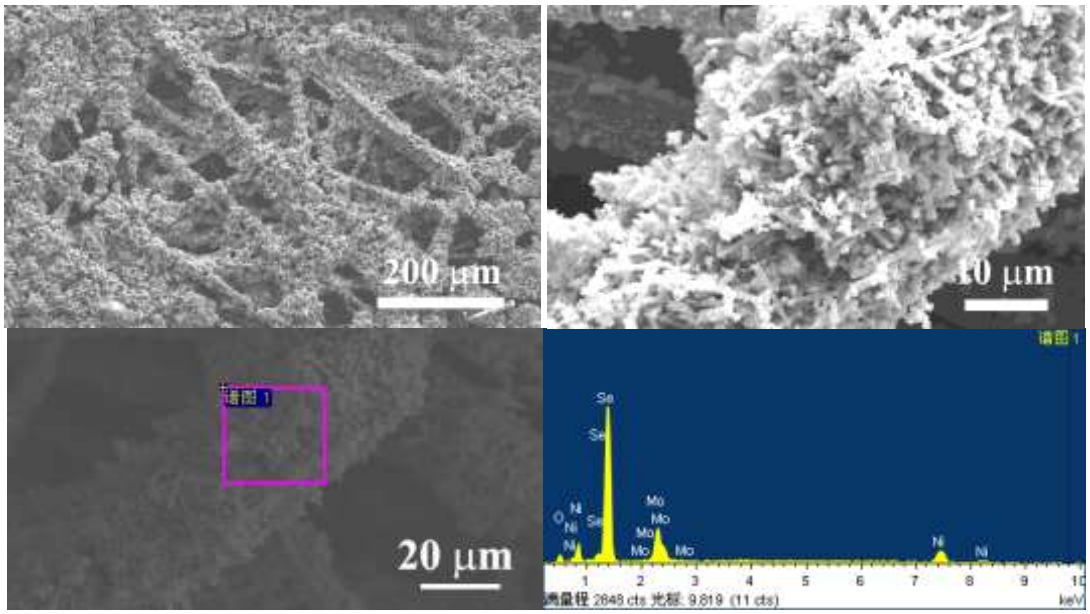

Figure S9. SEM image and EDS spectrum of SC-NiSe/$MoSe_2$@CFP

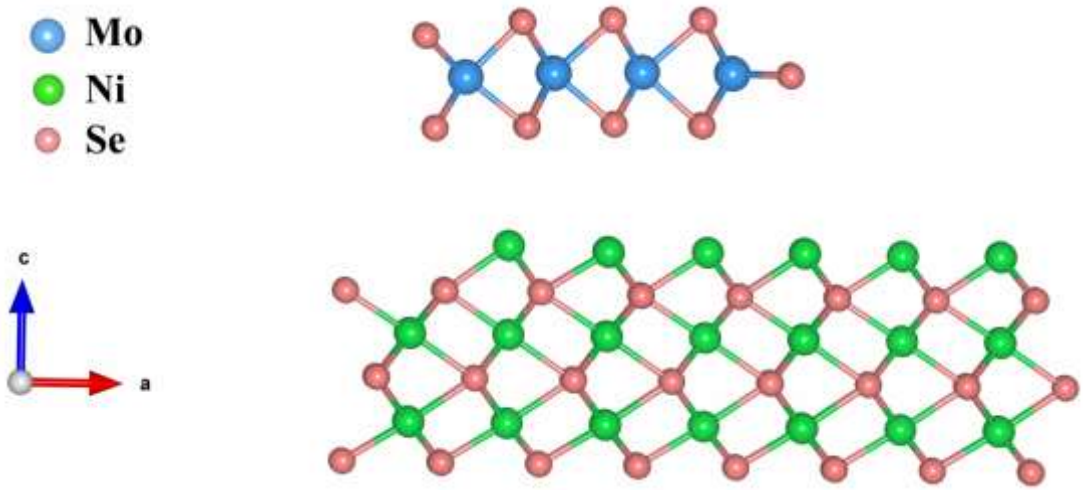

Figure S10. The structural models of the NiSe/$MoSe_2$ catalyst.

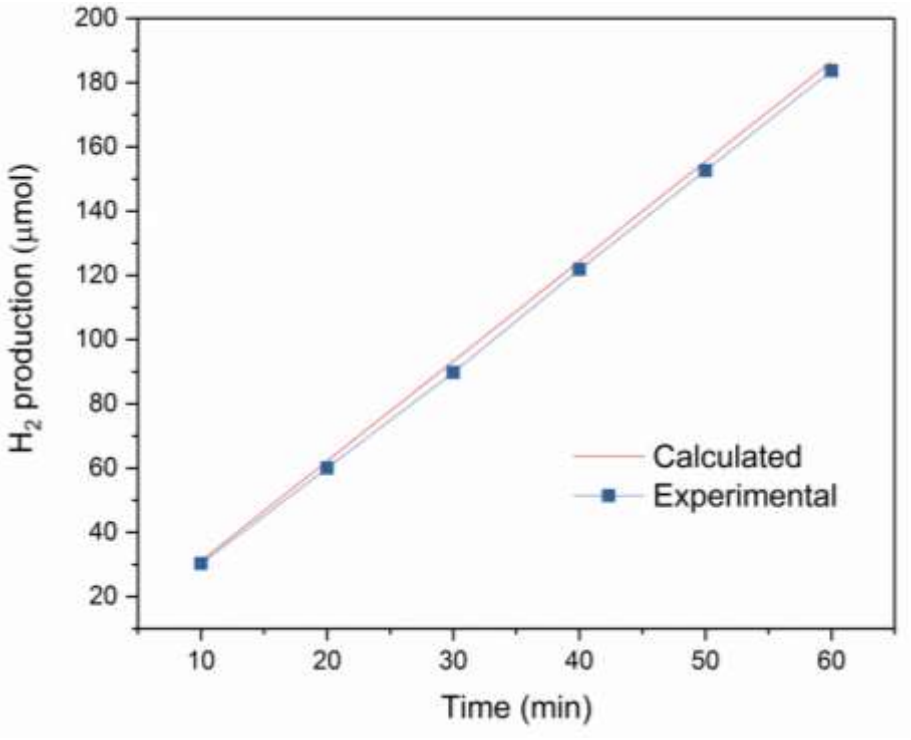

Figure S11. Faradaic efficiency of SC-NiSe/$MoSe_2$@CFP (at current of 10 mA)

Faradaic efficiency can be calculated: Faradaic efficiency = 2 F × $n_{(H2)}$ / Q, F is Faraday constant.

Table S2 Comparison on HER catalytic performance of recently reported electrodes

Sample	η @ j = -10 mA/cm2 or -100 mA/cm2 (mV)	Tafel slope (mV/dec)	Loading value mg/cm^2	Electrolyte	reference
SC-NiSe/$MoSe_2$@CFP	**71** (j = -10 mA/cm2) **129** (j = -100 mA/cm2)	/	**5**	**1.0 M KOH**	**This work**
MoS_2 /Ni_3S_2 @ Ni Foam	110 (j = -10 mA/cm2)	83.1	/	1.0 M KOH	*Angew. Chem. Int. Ed.* **2016**, *55*, 6702–6707.
$NiCo_2S_4$ nanowires array	210 (j = -10 mA/cm2)	58.9	/	1.0 M KOH	*Adv. Funct. Mater.*, **2016**, 26, 4661–4672.
NiS_2/MoS_2 nanowires array	> 76 (j = -10 mA/cm2) ~250 (j = -100 mA/cm2)	70	/	1.0 M KOH	*J. Mater. Chem. A*, **2016**, 4, 13439–13443.
$NiMoS_4$ nanoarray	191 (j = -100 mA/cm2)	97	1.7	1.0 M KOH	*J. Mater. Chem. A*, **2017**, 5, 16585–16589.
Cu_3P nanosheets array	105 (j = -10 mA/cm2)	42	1.2	1.0 M KOH	*ACS Appl. Mater. Interfaces*, **2017**, 9, 2240–2248.
Fe doped CoP nanoarray	78 (j = -10 mA/cm2)	75	1.0	1.0 M KOH	*Adv. Mater.*, **2017**, 29, 1602441.
$MoNi_4/MoO_{3-x}$ nanorod array	17 (j = -10 mA/cm2) 52 (j = -100 mA/cm2)	36	8.7	1.0 M KOH	*Adv. Mater.*, **2017**, 29, 1703311.
MoS_2/Ni_3S_2 nanorods	98 (j = -10 mA/cm2) 191 (j = -100 mA/cm2)	61	13	1.0 M KOH	*ACS Catal.*, **2017**, 7, 2357–2366.
$Ni(OH)_2$-Ni_3N nanoarray	181 (j = -100 mA/cm2)	86	3.2	1.0 M KOH	*J. Mater. Chem. A*, **2018**, 6, 833–836.
$Ni(OH)_2$-FeP nanoarray	76 (j = -10 mA/cm2)	105	1.34	1.0 M KOH	*Chem. Commun.*, **2018**, 54, 1201–1204.
Ni-Co-A nanosheets array	58 (j = -10 mA/cm2)	57	0.28	1.0 M KOH	*J. Am. Chem. Soc.*, **2018**, 140, 5241–5247.

References

1. Kresse, G.; Hafner, J. Ab initiomolecular dynamics for liquid metals. *Phys. Rev. B* 1993, **47**, 558–561.
2. Kresse, G.; Furthmüller, J. Efficiency of ab-initio total energy calculations for metals and semiconductors using a plane-wave basis. *Comput. Mater. Sci.* 1996, **6**, 15–50.
3. Blöchl, P. E. Projector augmented-wave method. *Phys. Rev. B* 1994, **50**, 17953–17979.
4. Kresse, G.; Joubert, D. From ultrasoft pseudopotentials to the projector augmented-wave method. *Phys. Rev. B* 1999, **59**, 1758–1775.
5. Perdew, J. P.; Burke, K.; Ernzerhof, M. Generalized Gradient Approximation Made Simple. *Phys. Rev. Lett.* 1996, **77**, 3865–3868s.
6. J. K. Nørskov, T. Bligaard, A. Logadottir, J. R. Kitchin, J. G. Chen, S. Pandelov and U. Stimming, *J. Electrochem. Soc*., 2005, **152**, J23.
7. J. K. Nørskov, J. Rossmeisl, A. Logadottir, L. Lindqvist, J. R. Kitchin, T. Bligaard and H. Jónsson, *J. Phys. Chem. B*, 2004, **108**, 17886–17892.